PERGAMON

International Journal of Heat and Mass Transfer 45 (2002) 597–607

International Journal of HEAT and MASS TRANSFER

www.elsevier.com/locate/ijhmt

A study of $CaCO_3$ fouling with a microscopic imaging technique

Won Tae Kim [a], Cheolho Bai [a,b], Young I. Cho [a,*]

[a] *Department of Mechanical Engineering and Mechanics, Drexel University, Philadelphia, PA 19104, USA*
[b] *Department of Mechanical Engineering, Yeungnam University, Republic of Korea*

Received 5 May 2000; received in revised form 23 April 2001

Abstract

The present study introduces a new experimental method to visualize the fouling process of $CaCO_3$. A mini-channel heat exchanger system with a microscopic imaging technique was developed for real-time visualization of the fouling process. The present study discussed how scale started initially, how scale formed thick layers, and how a small crystal grew into a large one, touching the adjacent one. Detail microscopic images of scale crystals and corresponding fouling resistances were obtained over the entire fouling process. The microscopic observation indicated that the fouling process could be divided into three stages: an induction period, a period of uniform generation of nuclei, and a period of uniform growth of scale. Sudden appearance of numerous small nuclei indicated the end of the induction period, a key event before the rapid increase in the fouling resistance. The present experimental method using microscopic images of the wet fouling process provides a valuable insight on the fouling mechanism.

1. Introduction

Scale is formed when hard water is heated (or cooled) in heat-transfer equipment such as heat exchangers, condensers, evaporators, cooling towers, boilers, and pipe walls. The type of scale differs depending on the mineral content of the available water. Scale often observed in industry includes calcium carbonate, calcium sulfate, barium sulfate, silica, iron scales, and others. One of the most common forms of scale is calcium carbonate ($CaCO_3$), which occurs naturally as an ingredient of chalk, limestone, and marble. Acidic water passing over and permeating through the ground dissolves limestone into calcium and bicarbonate ions, thereby making hard water. When the hard water is heated inside heat-transfer equipment, the calcium and bicarbonate ions precipitate due to the changes in solubility, forming hard scale on the heat-transfer surfaces, and clogging pipes and manifolds. When scale deposits in a heat exchanger surface, it is traditionally called fouling [1–3].

Fouling on a heat-transfer surface reduces the performance of a heat exchanger. The effects of temperature and flow velocity on fouling resistance have been extensively studied, from which the fouling mechanisms were speculated or modeled [3–5,8–11]. To understand the behavior of the fouling, researchers [1–8] measured the fouling resistance as a function of time. The analytic [1,3–6] and semi-analytic [2] models were developed based on these experimental studies to estimate fouling resistance in the heat exchanger. These models did not always give good agreement with experimental results.

Hasson et al. [4] presented a fouling model to predict the fouling rate in a heat exchanger considering $CaCO_3$ deposition only. Since their analytical model did not consider the removal mechanism, the model is applicable to low velocity flows where the removal process is negligibly small. Mattias-Bohnet [5] developed a fouling model by employing a mean crystal size in the fouling layer since the crystal size could not be determined during a fouling process. Their physical model for

* Corresponding author. Tel.: +1-215-895-2425; fax: +1-215-895-1478.
E-mail address: choyi@drexel.edu (Y.I. Cho).

0017-9310/02/$ - see front matter
PII: S0017-9310(01)00166-1

Nomenclature

A	Heat-transfer surface area (m^2)
D_h	Hydraulic diameter (m)
h	Convective heat-transfer coefficient (W/m^2 K)
l_e	Entrance length (m)
Nu	Nusselt number
Pr	Prandtl number
Q	Heat-transfer rate (W)
Re	Reynolds number
R_f	Fouling resistance (m^2 K/W)
T	Time
T_b	Bulk temperature (°C)
T_s	Surface temperature (°C)
U_{ini}	Initial overall heat-transfer coefficient (W/m^2 K)
U_{fouled}	Fouled overall heat-transfer coefficient (W/m^2 K)

crystallization fouling started with a thin fouling layer from the beginning of a fouling process, thus not considering the induction period often observed in many fouling processes.

Yiantsios et al. [9] pointed out the need to further improve such a fouling model by considering the effect of various crystalline phases on the deposit. The crystals were characterized by different cohesiveness and strength properties, and consequently by different resistances to detachment. Yiantsios et al. [9] concluded that the fouling resistance strongly depended on the characteristics of the deposit layer. Therefore, it would be useful to visualize the time-dependent morphology and properties of the deposit layer in terms of operating conditions and water qualities.

Accordingly, the present study attempted to document the crystallization fouling process of $CaCO_3$ on a wet surface of a heat exchanger through microscopic observation by photographically recording the entire fouling process including the inception of nucleation, crystal growth, scale-layer formation, and scale removal. By visually documenting the entire fouling process using a microscope, one could better understand how scale starts initially, how scale forms thick layers, and how a small-scale crystal grows into a large one, touching the adjacent one. Such information can be useful in considering how fouling can be mitigated and prevented.

2. Experimental method

In order to obtain real-time visualization as the fouling progressed, a fouling-test facility with a mini-channel heat exchanger and a microscopic imaging system was developed. Fig. 1 shows a schematic diagram of a once-through fouling-test loop, which consisted of two cooling-water tanks, a hot-water supply system, a microscopic imaging system, and a main fouling-test section. The hot-water supply system consisted of a 24 kW electric heater and a steam separator. Tap water was

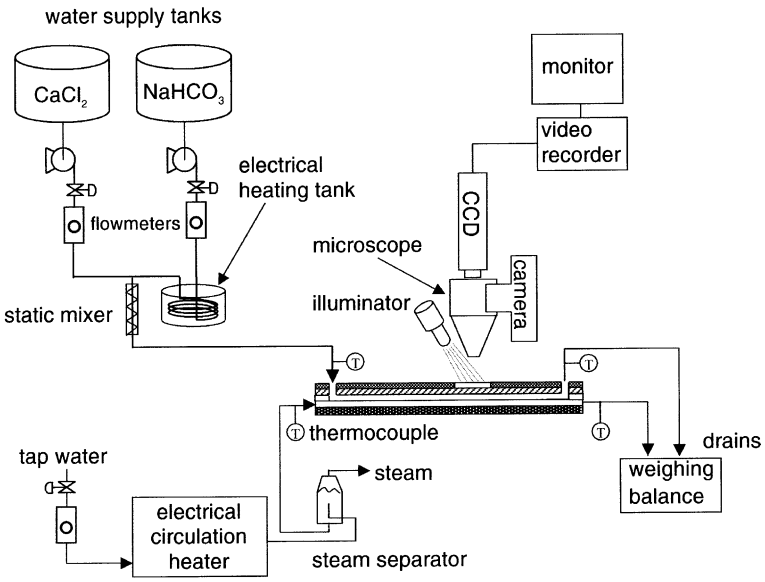

Fig. 1. Schematic diagram of the present experimental system.

electrically heated to 94°C and entered the hot-water channel of the main test section. The steam separator was used to eliminate steam bubbles from the hot water produced in the electric heater because bubbles were found to attach on the heat-transfer surface of the hot-water channel and significantly affect the outcome of the fouling experiment. The flow rate of the hot water was maintained at 2.6×10^{-5} m^3/s.

The microscopic imaging system consisted of a microscope, an external illuminator, a Sony charged couple device (CCD)-IRIS camera, a 35-mm Nikon camera, a video recorder, and a monitor. The images of $CaCO_3$-scale crystals on the cooling-water side were observed using the microscope and continuously recorded in videotape using the CCD camera. The objective lens of 40× was used for observation. Still pictures were taken with the 35-mm camera.

Fig. 2 shows cross-sectional views of the test channel including the microscopic view window position, which consisted of a copper plate as the heat-transfer surface, a cooling-water channel (i.e., the upper part of the flow channel), and a hot-water channel (i.e., the lower part of the flow channel). Cooling water moved in opposite directions to hot water, thus forming a counter-flow heat exchanger.

Because of the inverse-solubility characteristics of calcium carbonate salt, $CaCO_3$ scale was deposited on the cooling-water side of the copper plate. A new copper plate was used for each test. For the cooling-water channel, the two sidewalls were made of polypropylene plates whereas the top wall was made of a transparent acrylic plate due to its excellent clarity and thermal insulation. The hot-water channel was machined out of a Teflon block. The dimension of the cooling-water channel was 1.6 mm

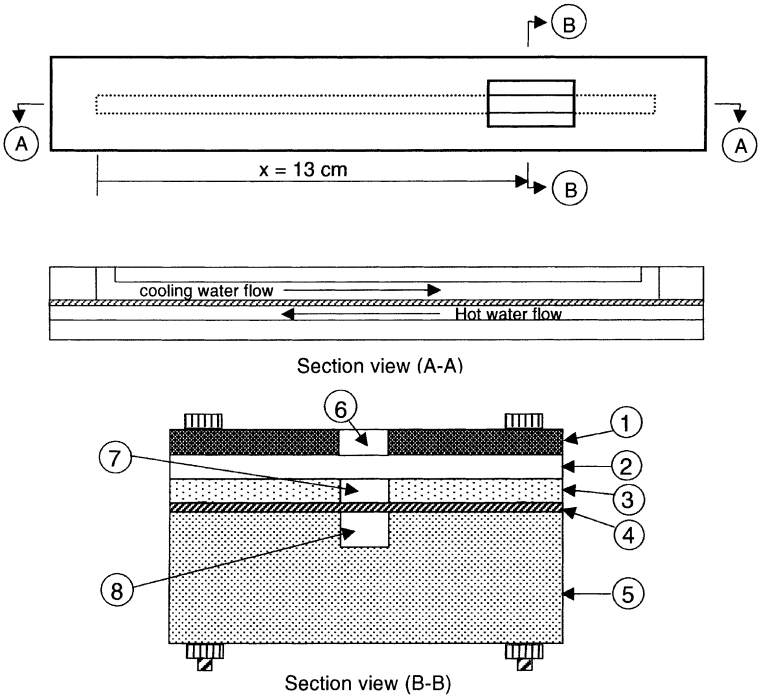

#	materials	properties	maximum allowable temp. (°C)
1	metal		
2	acrylic	excellent optical clarity	82
3	polypropylene	excellent thermal insulation	108
4	copper	heat transfer surface	
5	teflon	excellent thermal insulation	262
6	observation window		
7	flow channel for cooling (hard) water		
8	flow channel for hot water		

Fig. 2. Cut-away view of a mini-channel heat exchanger.

$\times$6.4 mm $\times$ 254 mm (height$\times$ width $\times$ length), whereas the dimension of the hot-water channel was 3.7 mm $\times$ 6.4 mm $\times$ 254 mm (height$\times$ width $\times$ length).

The cross-sectional view of the test section is shown in Fig. 2, where the counter flow was clearly indicated by two arrows indicating cooling and hot water flows. The location of the viewing port was 13 cm from the inlet of the cooling channel, where the flow was fully developed. The entrance length in the present heat-transfer test section was about 5 cm from the inlet of the cooling channel, which was calculated using the following equation [12]

$$\frac{l_e}{D_h} = 4.4 Re^{1/6}. \quad (1)$$

The cooling water was artificially hardened with $CaCl_2$ and $NaHCO_3$ prepared in two separate tanks. One tank contained 0.0075 M calcium chloride ($CaCl_2$) solution, and the other contained 0.015 M sodium bicarbonate ($NaHCO_3$) solution. The solution from each tank was pumped individually and mixed through a static mixer before entering the main fouling-test section. The mixed solution was equivalent to hard water of 750 ppm as $CaCO_3$. Durations of fouling tests were between 6 and 11 h, which varied depending on flow velocity.

Two different velocities of cooling water (i.e., 1.2 and 2.5 m/s) were used in the present study, and the corresponding Reynolds numbers were 5060 and 9600, respectively, based on the hydraulic diameter of the flow channel. The inlet temperature of the cooling water varied from 30°C to 55°C, so that one could examine the effect of the cooling-water temperature on the fouling process. The inlet and outlet temperatures of the hot water were maintained at 94°C and 90°C, respectively, throughout the entire experiment. T-type thermocouples were used to measure the inlet and outlet temperatures of both cooling water and hot water. Flow rates of both cooling water and hot water were measured by rotameters (Omega Engineering), which were calibrated using a precision weighing balance. Temperature probes were not used on the heating surface because they could have disturbed the flow in the narrow flow channel. The convective heat-transfer correlation in a one-side heated rectangular pipe [13] was given by the following equations

$$Nu = 0.79 Re^{0.4} Pr^{0.52}, \quad (2)$$

$$Q = hA(T_s - T_b). \quad (3)$$

The average surface temperature of the copper plate for all runs was estimated to be 66 ± 2°C using Eqs. (2) and (3). Fouling resistance was estimated by the following equation [14]

$$R_f = \frac{1}{U_{fouled}} - \frac{1}{U_{ini}}, \quad (4)$$

where U_{ini} and U_{fouled} are the overall heat-transfer coefficients at the initial time and at $t \geqslant 0$, respectively. The overall heat-transfer coefficient, U, was calculated using the log-mean-temperature-difference (LMTD) method, based on four temperatures at both inlet and outlet of cold and hot flow channels.

To estimate the uncertainty in experimental results, a method presented by Kline and McClintock [15] was used, which is based on the uncertainty in various primary experimental measurements such as flow rate and temperature. The basic uncertainties of a surface area, a temperature, and the flow rate of cold water were found to be $\pm 0.8\%$, $\pm 0.35\%$, and $\pm 0.3\%$, respectively. The uncertainties for the overall heat-transfer coefficient and fouling resistance were estimated to be 2.3% and 10%, respectively.

3. Results

Fig. 3 presents a series of photographs showing the entire fouling process for the severe-fouling case of an inlet-cooling-water temperature of 55°C and a velocity of 1.2 m/s. The alphabetical letters (A–H) indicate various states that are also marked in Fig. 9 for cross-reference. The results shown in Fig. 3 reveal that from the beginning, i.e., $T = 0$ and 30 min, there were already numerous small crystals whose sizes were about 90 μm. As fouling progressed, these small crystals rapidly grew up to 160 μm, covering the entire heat-transfer surface at $T = 2$ h.

Fig. 4 presents another series of photographs showing the fouling process for the case of an inlet temperature of 38°C and a velocity of 1.2 m/s. The only difference from the case shown in Fig. 3 was a reduced inlet temperature of the cooling water. As shown in Fig. 4, the crystal-growth patterns in the first 2 h were very different from those shown in Fig. 3. At the beginning of the fouling process (i.e., $T = 0$ and 30 min), the heat-transfer surface remained relatively scale free.

Fig. 5 shows the distribution of crystals whose sizes are equal to or greater than 60 μm. The number of crystals for the case of 55°C was 142 at $T = 30$ min, whereas the number of crystals for the case of 38°C was 60 at the same time. We speculate that these crystals formed in the beginning were created mainly due to the imperfect surface conditions of the new copper plate. A clean heat-transfer surface, perfectly smooth to naked eyes, often has cavities, scratches, or impurities like foreign particles when viewed via a microscope. In particular, foreign particles are likely to settle down in the cavity and become the initial nucleation sites for crystallization fouling. However, once a small number of $CaCO_3$ crystals were formed, these crystals began to grow rapidly, leaving the adjacent scale-free heat-transfer surface clean for a while. Fig. 4 shows that the clean scale-free surface between the crystals remained clean

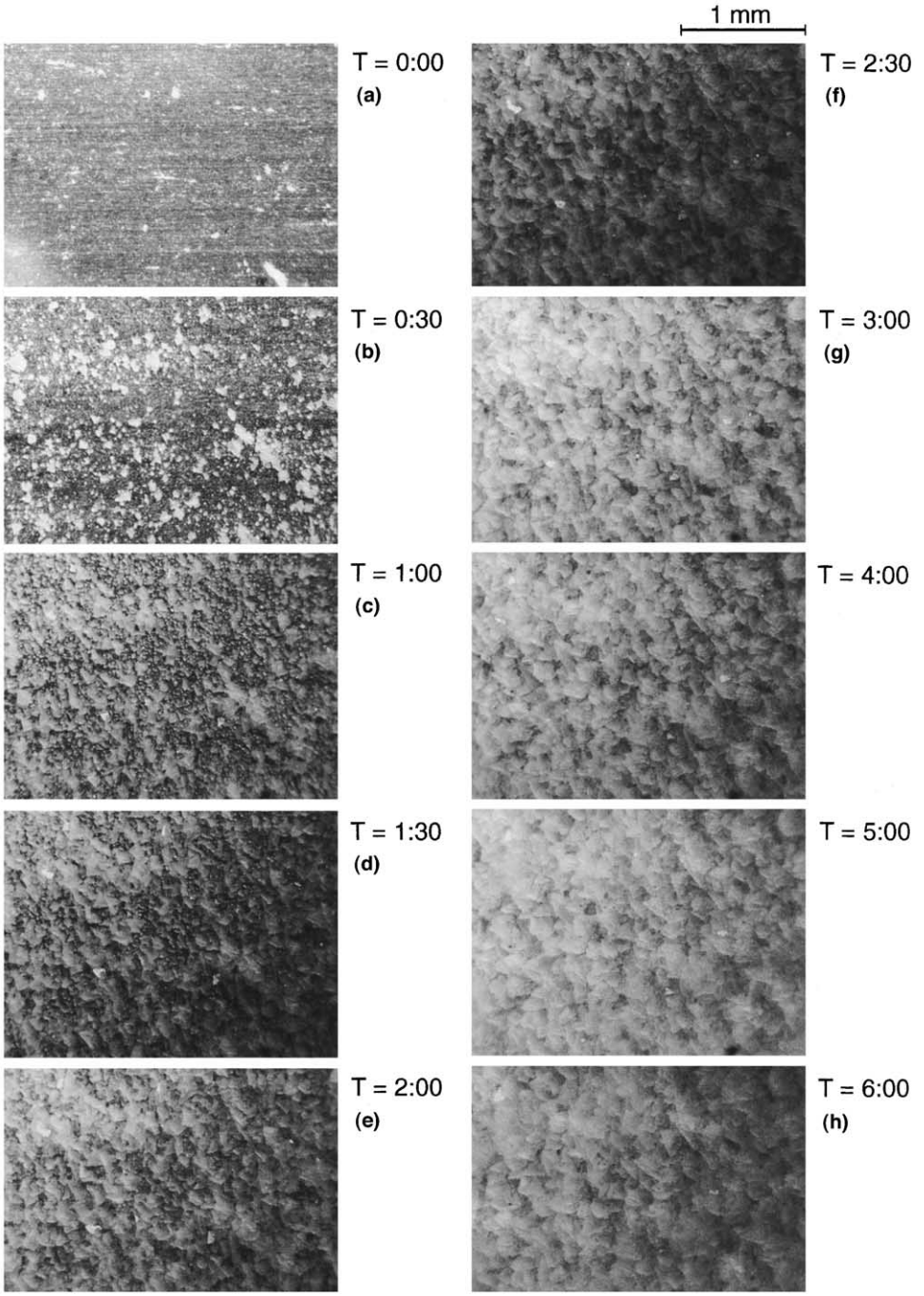

Fig. 3. Time-history microphotographs at inlet bulk temperature of 55°C and velocity of 1.2 m/s (Run 27). Magnification = 40×.

during the induction period of 1 h. The crystals present at $T = 30$ min grew sufficiently large such that they began to touch each other, covering the entire heat-transfer surface by $T = 3$ h (see Fig. 4).

Fig. 6 presents another series of photographs showing crystal-growth patterns for the case of an inlet-cooling-water temperature of 38°C and a velocity of 2.5 m/s. In comparison with the results given in Figs. 4 and 6, the increased flow velocity clearly suppressed the generation of $CaCO_3$ crystal during first 3 h. For example, for the case of the increased flow velocity of 2.5 m/s, there were only six relatively large sized crystals in

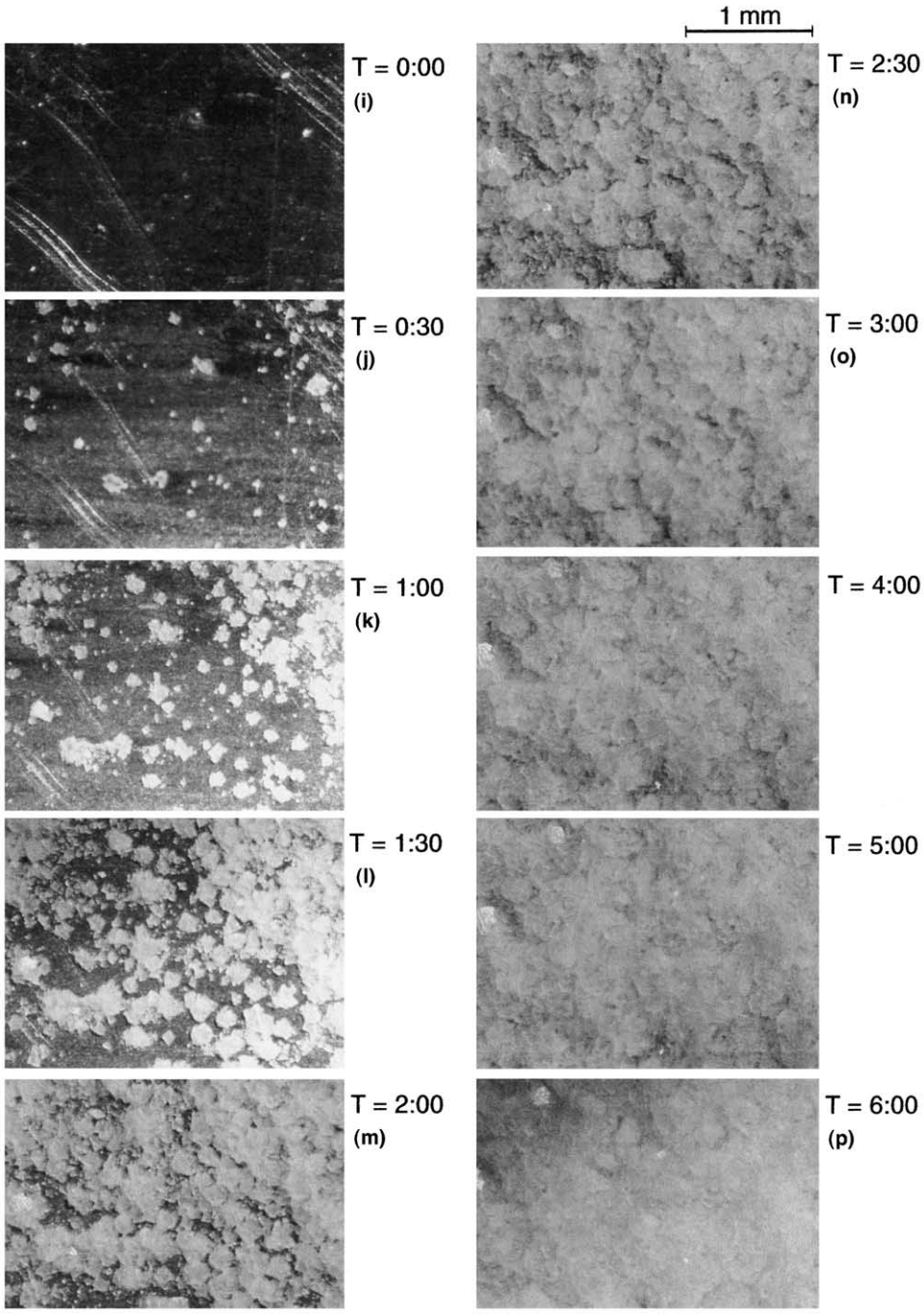

Fig. 4. Time-history microphotographs at inlet bulk temperature of 38°C and velocity of 1.2 m/s (Run 29). Magnification = 40×.

the range of 130–300 μm at $T = 3.5$ h (see Fig. 6), whereas for the case with 1.2 m/s there were numerous $CaCO_3$ crystals at $T = 3$ h (see Fig. 4).

For the case of 2.5 m/s, new small crystals began appearing between large $CaCO_3$ crystals at $T = 3.5$ h (see Fig. 6), and they were numerous and became clearly visible at $T = 4$ h. This moment – when many tiny new crystals suddenly appear between large crystals – is defined as the end of the induction period and the beginning of the next stage, a subject that will be further discussed later in relation to the fouling curve in Fig. 9. Once numerous small crystals began to be formed at

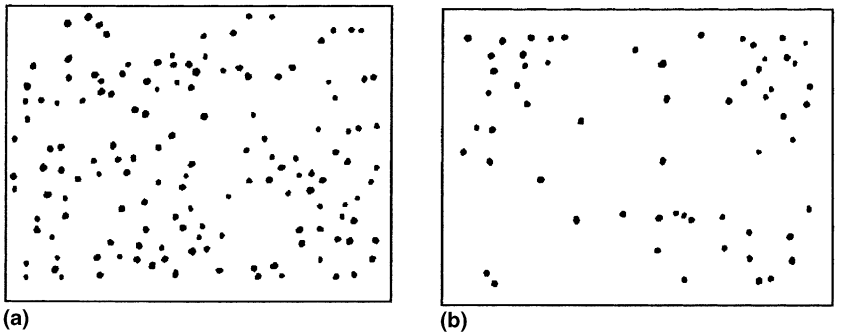

Fig. 5. Population of crystals at 30 min. (a) Run 27: 55°C and 1.2 m/s (number of crystals = 142 at 30 min); (b) Run 29: 38°C and 1.2 m/s (number of crystals = 60 at 30 min).

$T = 3.5$ h, these crystals began to rapidly grow and eventually covered the entire heat-transfer surface within 1 h at $T = 4.5$ h as shown in Fig. 6.

Fig. 7 presents another series of photographs showing the fouling process for the case of an inlet-cooling-water temperature of 30°C and a velocity of 2.5 m/s. At this reduced cooling-water temperature and increased velocity, $CaCO_3$ crystals were hardly created even in the artificially harsh condition of 750 ppm as $CaCO_3$. Due to the high shear stress corresponding to the velocity of 2.5 m/s, the heat-transfer surface kept almost clean for the first 8–9 h. At $T = 8$ h, there was a very big crystal of 680 μm, which had grown from a small nucleation site. Once a nucleation took place in a high shear environment, the seed nucleation grew into a very big crystal compared to the crystals for higher temperature and/or lower velocity.

Fig. 7 clearly reveals that as calcium ions precipitated due to a sudden drop in the solubility inside the test section, they were attracted by the calcium carbonate surface, thus feeding almost exclusively the $CaCO_3$ crystal while leaving the scale-free heat-transfer surface clean for a while. Crystals identified as #2–#5 at $T = 11$ h had grown from small seed crystals seen at $T = 9$ h. The observation that the existing crystals continued to grow rather than the creation of new seed crystals has been reported in the literature [16–18]. For example, precipitating calcium ions prefer the calcium carbonate surface to the metal-heat-transfer surface due to the lower Gibbs free energy of the crystal lattice [16] and/or higher mass transfer toward the surface of crystals [17]. Furthermore, the surface of crystal itself becomes nucleation sites [18].

Fig. 8 shows the growing rates of the six crystals identified at the bottom of Fig. 7. It is interesting to note that all six crystals grew at almost the same rate. The previous study [19] revealed that crystals formed earlier grew faster than the ones formed later since the bigger crystals attract precipitating calcium ions, thus suppressing the growth rate of adjacent small crystals. In the present study, as one small seed crystal grew to a large one for the first 8 h, no other crystals could be formed around it. Small crystals were finally formed after $T = 8$ h and began to grow at the same rate as the one large crystal formed much earlier. We speculate that when the big crystal grows to a certain size, it does not attract precipitating calcium ions as much as it did before, thus allowing other small seed crystals to be formed and to grow. In this situation, the growth rates of the big one formed early and small ones formed much later become almost identical. In all photographs given Figs. 3, 4, 6 and 7 as well as the images recorded in videotapes, crystals had rounded shapes, indicating mostly calcite crystals, not needle-shaped aragonite crystals.

Fig. 9 shows the fouling resistance vs. time curves for four different test conditions. The alphabetical letters (A–H, I–P, a–e, and f–j) are marked in Fig. 9 to assist in comparing the fouling resistance curves with photographs in Figs. 3, 4, 6 and 7. For the most severe-fouling condition, Run 27, the fouling resistance began increasing from the beginning without an induction period. The rate of fouling (i.e., slope) somewhat decreased between points B and D due to an initial scale buildup and increased again from point D almost linearly with time.

For Run 29, the fouling resistance remained almost zero for the first 1 h (see points I, J, and K) and began rising from point K continuously. The slope for Run 29 was much smaller than that for Run 27, indicating that the low cooling-water temperature reduced the fouling rate. For Run 31, the fouling resistance was practically zero for the first 3.5 h (see points a and b). Beyond $T = 3.5$ h, the fouling resistance increased almost linearly with time. For Run 33, the fouling resistance was almost zero for the first 4 h and began increasing very slowly beyond that.

4. Discussion

The present study examined the relationship between the fouling resistance and characteristics of scale

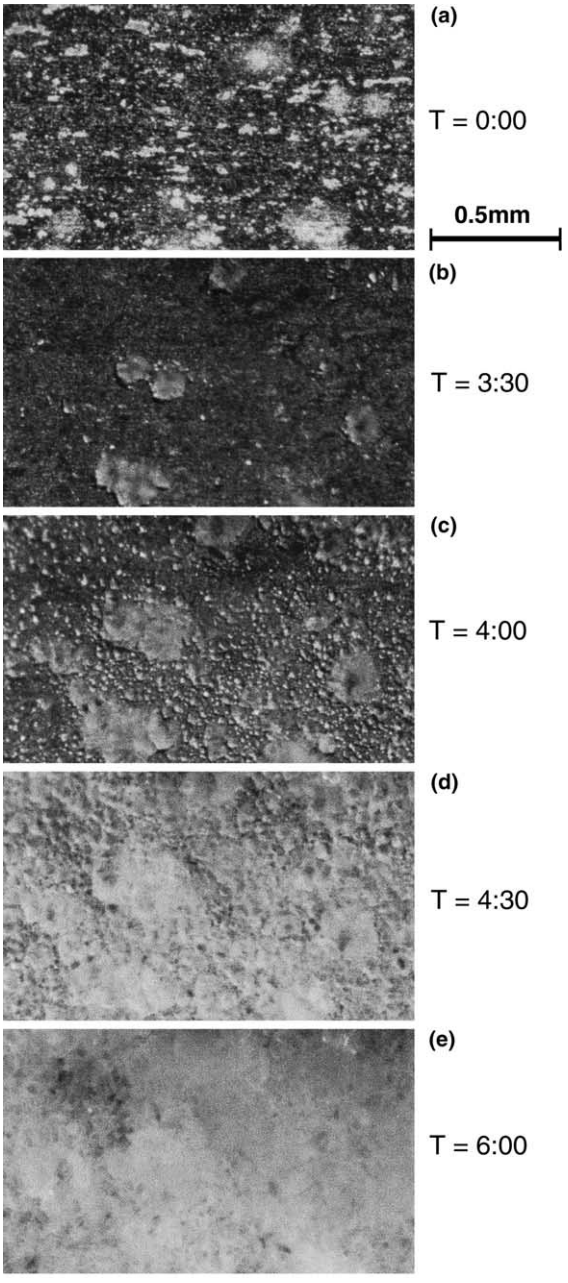

Fig. 6. Time-history microphotographs at inlet bulk temperature of 38°C and velocity of 2.5 m/s (Run 31). Magnification = 40×.

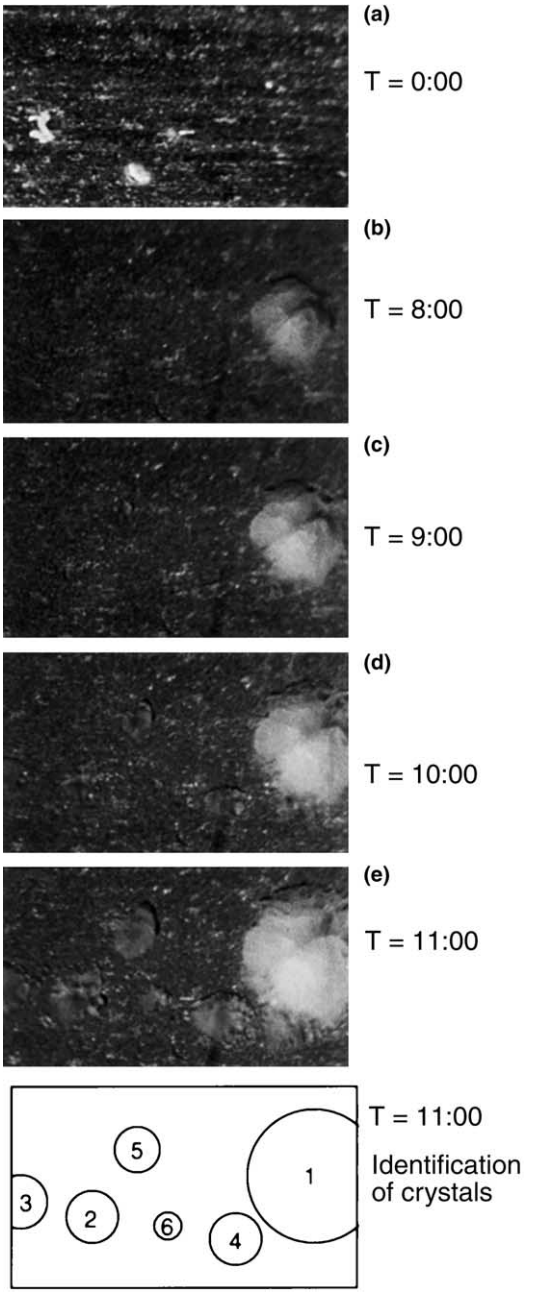

Fig. 7. Time-history microphotographs at inlet bulk temperature of 30°C and velocity of 2.5 m/s (Run 33). Magnification = 40×.

formation during the induction period and a period of subsequent scale growth. Chuanfang [20] described the induction period as the duration when growing crystals interlinked, forming an extremely thin layer on the heat-transfer surface. Budair et al. [21] defined the induction period as the onset time of scaling. Based on the present observation, the induction period can be practically defined as the period when crystals continue to grow but the heat-transfer is not reduced. The present results confirmed that the induction period was strongly affected by the inlet-cooling-water temperature and flow velocity. The induction periods for the four different cases in the present study (i.e., Runs 27, 29, 31, and 33)

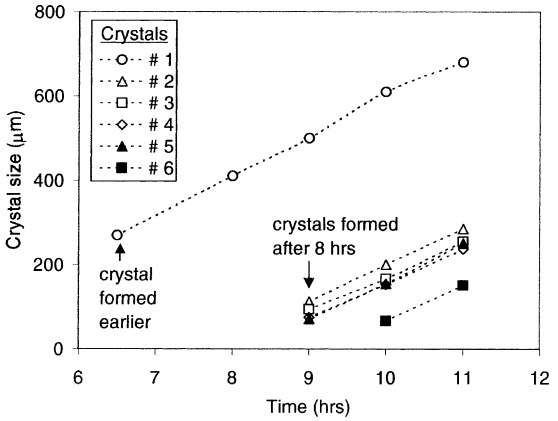

Fig. 8. Size of crystal growth in Run 33.

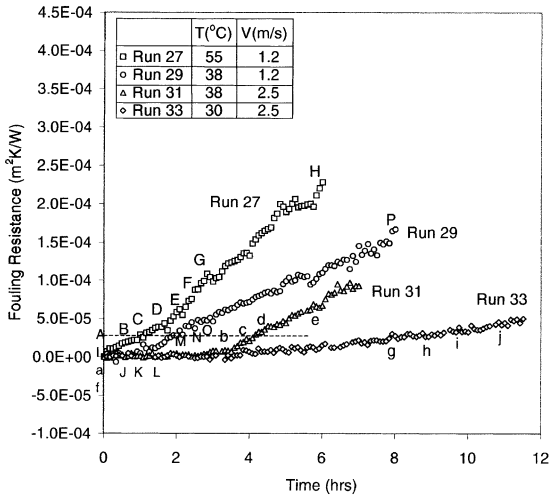

Fig. 9. Fouling resistance curves over time for four different runs.

were determined to be 0, 1, 3, and 3.5 h (see Figs. 3, 4, 6 and 7), respectively.

After the induction period, small nuclei began to uniformly appear in spaces between large crystals all over the heat-transfer surface. Consequently, the fouling resistance began to increase rapidly as depicted by the results in Fig. 9. The uniform generation of small nuclei turned out to be the key event before the rapid increase in the fouling resistance, whereas large crystals generated during the induction period did not increase the fouling resistance. For example, the small nuclei began to appear on the heat-transfer surface at $T = 0$, 1, and 3 h for Runs 27, 29, and 31, respectively. These events exactly matched with the moment when the fouling resistance curves began to rise.

The present results depicted that the population of the nuclei strongly depended on the experimental conditions. For example, the case of an inlet temperature of 55°C and a velocity of 1.2 m/s in Fig. 3 shows substantially more nuclei at $T = 0.5$ h than the case of an inlet temperature of 38°C and a velocity of 1.2 m/s (see Fig. 4 at $T = 1.5$ h). As the population of the nuclei increased, the scale on the heat-transfer surface became crowded, and the crystals were generally small in size. Similar behavior can be seen for an increased velocity of 2.5 m/s from Figs. 6 and 7, i.e., the case with a high temperature cooling water generated more nuclei than the case with a low temperature one.

Most previous fouling studies examined the scale structure at the end of fouling tests so that they did not have an opportunity to see how the final scale structure was obtained. The present study attempted to produce new knowledge on the precipitation fouling by revealing the fouling history. For instance, for the case of a high bulk temperature of cooling water, numerous nucleation sites were formed on a heat-transfer surface in the beginning stage of the fouling process. In contrast, for the case of a low bulk temperature of cooling water, much smaller numbers of nucleation sites were formed com-

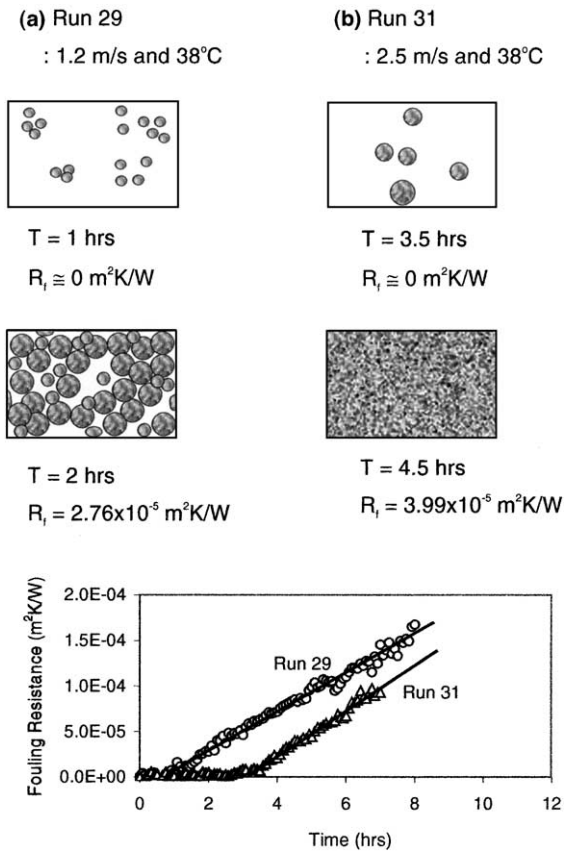

Fig. 10. Photograph images vs. fouling resistance for the case of different velocities in Runs 29 and 31.

pared to the case of the higher bulk temperature. However, when one compares the final scale structures for both cases at the end of fouling tests, one could not see this important distinction.

Although Figs. 3, 4, and 6 show different patterns of crystal formation in terms of crystal size and population, fouling resistances were almost identical (see a dashed line in Fig. 9) at the very moment when the heat-transfer surface was fully covered by scale (i.e., $T = 1$, 2, and 4 h for Runs 27, 29, and 31, respectively).

The effect of the flow velocity on the fouling rate is one of the confusing issues in fouling research. Generally, most field engineers assume that the increase in the flow velocity should result in a reduced fouling rate. When one compares the slopes in Fig. 9 (i.e., the rate of fouling resistance) for Runs 29 and 31, the high flow velocity case (Run 31) shows a steeper slope than that in the lower velocity case of Run 29.

Fig. 10 shows a relationship between photographic images of fouled surfaces and fouling resistances for two different velocities in Runs 29 and 31. The induction periods for the two cases were 1 and 3.5 h, respectively. Clearly, the induction period is lengthened with increasing flow velocity. The issue at hand is how the fouling rate is affected by flow after the induction period. The fouling resistances 1 h after the completion of the induction period (i.e., $T = 2$ and 4.5 h) were 2.76×10^{-5} and 3.99×10^{-5} m^2 K/W for the two cases (i.e., 1.2 and 2.5 m/s), respectively. At the same time, the scale-crystal image at the 1.2-m/s case shows a partially clean surface, whereas the 2.5-m/s case shows a fully covered surface by crystals. Photographic images given in Fig. 10 clearly suggest that once the induction period is completed, the high flow velocity accelerates scale deposit, presumably due to an enhanced mass-transfer rate of precipitating calcium ions at the heat-transfer surface, resulting in a rapid increase in the fouling resistance.

5. Conclusions

A new experimental method was developed to investigate the fouling process by examining the entire history of scale formation using a microscopic observation. The fouling process was divided into three stages: an induction period, a period of the uniform generation of nuclei, and a period of rapid scale growth. The duration of the induction period was strongly affected by both the inlet temperature of the cooling water and flow velocity. The small nuclei suddenly appeared near the end of the induction period and grew rapidly with time, thus beginning to increase the fouling resistance. Although different test runs showed different patterns of crystal formation such as crystal size and population, almost the same fouling resistances were obtained at the moment when the heat-transfer surface was fully covered with $CaCO_3$ crystals. Once the heat-transfer surface is fully covered by the scale layer, the subsequent deposition takes place over the rough scaled surface, and the fouling process is accelerated by flow. The microscopic visualization method introduced in the present study can be useful in the further development of various scale-control technologies, both chemical treatment and non-chemical treatment such as permanent magnets and electronic-descaling technology.

Acknowledgements

C. Bai acknowledges the financial support (a research grant) from Yeungnam University, Korea during his sabbatical leave in 1999.

References

[1] D. Hasson, M. Avriel, W. Resnick, T. Rozenman, S. Windreich, Mechanism of calcium carbonate scale deposition on heat-transfer surface, Ind. Eng. Chem. Fund. 7 (1968) 58–63.

[2] J. Taborek, T. Aoki, R.B. Ritter, J.W. Palen, J.G. Knudsen, Predictive methods for fouling behavior, Chem. Eng. Prog. 68 (1972) 69–78.

[3] A.P. Watkinson, O. Martinez, Scaling of heat exchanger tubes by calcium carbonate, Trans. ASME 97 (1975) 504–508.

[4] D. Hasson, H. Sherman, M. Biton, Prediction of calcium carbonate scaling rates, in: Proceedings of 6th International Symposium Fresh Water from the sea, vol. 2, 1978, pp. 193–199.

[5] M. Bohnet, Fouling of heat transfer surfaces, Chem. Eng. Technol. 10 (1987) 113–125.

[6] S.H. Chan, K.F. Ghassemi, Analytical modeling of calcium carbonate deposition for laminar falling films and turbulent flow in annuli: Part 2 multispecies model, J. Heat Transfer 113 (1991) 741–746.

[7] T.R. Bott, The Fouling of Heat Exchangers, Elsevier Science, New York, 1995.

[8] H. Muller-Steinhagen, Cooling water fouling in heat exchangers, Advances in Heat Transfer, vol. 33, Academic Press, New York, 1999, pp. 415–496.

[9] S.G. Yiantsios, N. Andritsos, A.J. Karabelas, Modeling heat exchanger fouling: current status, problems and prospects, in: Proceedings of Fouling Mitigation of Industrial Heat-Exchange Equipment, An International Conference, San Luis Obispo, California, June 1995, pp. 337–351.

[10] J. Taborek, T. Aoki, R.B. Ritter, J.W. Palen, Fouling: the major unresolved problem in heat transfer, Chem. Eng. Prog. 68 (1972) 59–67.

[11] X. Dunqi, J.G. Knudsen, Functional correlation of surface temperature and flow velocity on fouling of cooling-tower water, Heat Transfer Eng. 7 (1986) 63–71.

[12] B.R. Munson, D.F. Young, T.H. Okiishi, Fundamentals of Fluid Mechanics, second ed., Wiley, New York, 1994, p. 460.

[13] W.M. Rohsenow, J.P. Hartnett, Y.I. Cho, Handbook of Heat Transfer, third ed., McGraw-Hill, New York, 1998, p. 5.107.
[14] B. Bansal, H. Muller-Steinhagen, Crystallization fouling in plate exchangers, J. Heat Transfer 115 (1993) 584–591.
[15] S.J. Kline, F.A. McClintock, Describing uncertainties in single-sample experiments, Mech. Eng. January (1953) 3.
[16] R.A. Dawe, Y. Zhang, Kinetics of calcium carbonate scaling using observations from glass micromodels, J. Pet. Sci. Eng. 18 (1997) 179–187.
[17] T.R. Bott, Crystallization Fouling – Basic Science and Models Fouling Science and Technology, Kluwer Academic Publishers, Boston, 1988, pp. 251–260.
[18] T.R. Bott, Aspects of crystallization fouling, Exp. Thermal Fluid Sci. 14 (1997) 356–360.
[19] W.T. Kim, Y.I. Cho, Experimental study of the crystal growth behavior of $CaCO_3$ fouling using a microscope, Exp. Heat Transfer 13 (2) (2000) 153–161.
[20] Y. Chuanfang, Mechanisms of calcium carbonate scaling during and post induction period, in: Proceedings of Fouling Mitigation of Industrial Heat-Exchange Equipment, An International Conference, San Luis Obispo, California, June 1995, pp. 275–286.
[21] M.O. Budair, M.S. Khan, S.M. Zubair, A.K. Sheikh, A. Quddus, $CaCO_3$ scaling in AISI 316 stainless steel tubes – effect of the thermal and hydraulic parameters on the induction period and growth rate, Heat Mass Transfer 34 (1998) 163–170.